Mon. Not. R. Astron. Soc. **000**, 1–9 (1994) Printed 1 February 2008 (MN LATEX style file v1.4)

Restrictions to the galaxy evolutionary models from the Hawaiian Deep Fields SSA13 and SSA22

J. A. L. Aguerri[1] & I. Trujillo[2]

1.-Astronomisches Institut der Universität Basel. Venusstrasse 7. CH-4102 Binningen. Switzerland.
2.-Instituto de Astrofísica de Canarias. E38200 La Laguna (Tenerife). Spain.

arXiv:astro-ph/0202423v1 22 Feb 2002

Accepted 0000 December 00. Received 0000 December 00; in original form 0000 October 00

ABSTRACT

Quantitative structural analysis of the galaxies present in the Hawaiian Deep Fields SSA13 and SSA22 is reported. The structural parameters of the galaxies have been obtained automatically by fitting a two–component model (Sérsic $r^{1/n}$ bulge and exponential disc) to the surface brightness of the galaxies. The galaxies were classified on the basis of the bulge-to-total luminosity ratio (B/T). The magnitude selection criteria and the reliability of our method have been checked by using Monte Carlo simulations. A complete sample of objects up to redshift 0.8 has been achieved. Spheroidal objects (E/S0) represent $\approx$ 33% and spirals $\approx$ 41% of the total number of galaxies, while mergers and unclassified objects represent $\approx$ 26%. We have computed the comoving space density of the different kinds of objects. In an Einstein–de Sitter universe a decrease in the comoving density of E/S0 galaxies is observed as redshift increases (a $\approx$ 30% less at z=0.8), while for spiral galaxies a relatively quiet evolution is reported. The framework of hierarchical clustering evolution models of galaxies seems to be the most appropriate to explain our results.

Key words: galaxies: distances and redshift—galaxies: evolution—galaxies: photometry—galaxies: fundamental parameters

1 INTRODUCTION

Achieving a good galactic evolutionary model is one of the challenges of present astronomy. The high quality of the Hubble Space Telescope (HST) data allows astronomers to study the evolution of galaxy morphology over a significant fraction of the age of the Universe, restricting the two main present theoretical frameworks of galaxy evolution: the monolithic collapse and the hierarchical clustering models.

The simplest models of galaxy evolution predict that massive elliptical galaxies formed at high redshift in a rapid collapse with a single burst of star formation (Eggen et al 1962; Larson 1975). Against this scenario, the hierarchical clustering models predict that the most massive objects form at late times via the merging of smaller subunits (White & Rees 1978; Kauffmann et al 1993). Each model has very different observational implications (e.g. Brinchmann et al 1998; Schade et al 1999; Fried et al 2001). Observational evidence has been found for both scenarios (see Schade et al 1999 and references therein), so that the dominant mechanism of galaxy evolution remains an open question.

Many attempts have been made to classify galaxies on HST deep images. Two families of methods are currently used: visual and automated classifications. Among visual classifications we mention analysis done by van der Bergh et al (1996, 2000) in the range $21<I_{814}<25$ at the Hubble Deep Field (HDF). They found that up to 30% of the galaxies were ellipticals, the remainder divided into 31% spirals and 39% unclassified. Possible differences in the morphologies of galaxies at high redshifts point to different the environmental conditions of these galaxies relative to the local ones. In particular, the merger rate could be very different. Le Fevre et al (1999) have found that the rate of mergers and interaction grows strongly with the redshift. Quantitative classification systems based on the study of the central concentration and asymmetry of the galaxian light (Abraham et al 1996) also obtained a high fraction of irregular and peculiar galaxies at high redshifts, finding only a 20% of elliptical fraction.

Most sophisticated classification systems based on the decomposition of the surface brightness profiles of galaxies into their structural components (bulge and disc mainly) have been applied during the last few years. This technique is used extensively for local galaxies (see Prieto et al 2001 and references therein) but the lower resolution at high redshift makes its application there more difficult . This quantitative classification method has the advantage that it gives information about each component of galaxies. This means that we can follow the evolution of different components (bulge and disc in spirals) as a function of redshift. Usu-

© 1994 RAS

ally, it is assumed that the same type of profiles which fit the light distribution of local galaxies also describe the light distribution of galaxies at higher redshift. Typically, Sérsic $r^{1/n}$ profiles are fitted to the surface brightness profiles of bulges and elliptical galaxies, and exponential profiles to the discs of Spiral galaxies (Marleau & Simard 1998, Schade et al 1996, 1999).

Using this decomposition technique on the HDF, Marleau & Simard (1998) found a substantially different result from those obtained by visual classifications. They found that only 8% (versus 30% for visual classifications) of the galaxy population down to $I_{814}(AB) = 26$ are spheroidal systems. Although quantitative methods have clear advantages over visual methods, they are not free from significant bias which affect the reliability of the physical properties obtained. In order to understand the big discrepancy pointing out in the previous analysis, it is crucial to remove the bias which are present in quantitative analysis methods.

In this paper, we examine the structural properties of the galaxies in two Hawaiian Deep Fields (SSA13 and SSA22) imaged by HST. Each of these fields is composed by 3 HST/WFPC2 fields. All the galaxies studied in these fields have spectroscopic redshifts, avoiding a strong source of uncertainty at the distance determination. Previous classification schemes of high redshift galaxies from HST images are compared with our results. In particular, we focus our attention on evaluating the number of spheroidal systems in field galaxies and on constraining the two main theoretical frameworks of galaxy evolution.

The structure of this paper is as follow: section 2 describes the characteristics of the observed fields. The structural decomposition method is presented in section 3. In section 4 we discuss the completeness of the sample and we summarize our conclusions and discuss their implications for galaxy evolution in sections 5 and 6.

2 THE SAMPLE OF GALAXIES

The sample consists on all objects with K<20, I<22.5 (Kron-Cousins) and B<24.5 in two areas surrounding the Hawaii deep survey fields SSA 13 and SSA 22 (Cowie et al 1994; Songaila et al 1994). Hereafter, the I magnitude will be given in the same system as in Cowie et al (1996). Nearly all objects included in those fields have measured spectra with the LRIS spectrograph on Keck (Cowie et al 1996) ⋆. The fields were imaged during 2000 s with the WFPC2 at HST in the I_{814} bandpass. The total analyzed sky area was 28 arcmin^2. The analyzed objects lie in the redshift interval $[0.1, 1.3]$, mainly concentrated around $z = 0.5$ (see Cowie et al 1996).

We used the SExtractor galaxy photometry package (Bertin & Arnouts 1996, version 2.1.4) for the extraction of the objects from the public released HST images. This package is optimized to detect and measure sources from astronomical images. The detection was run using the same parameters as in Marleau & Simard (1998). In particular, we used a detection threshold of 1.5 σ, where σ is the standard deviation of the sky background of the images. Another important parameter is the deblending parameter. SExtractor deblends objects using multiple flux thresholding. The SExtractor deblending parameter sets the minimum fraction of the total flux a branch must contain to be considered a separate object. We have use the same value that Marleau & Simard (1998), which is 0.001.

⋆ See the discussion about the different magnitudes and transformations in Cowie et al (1995)

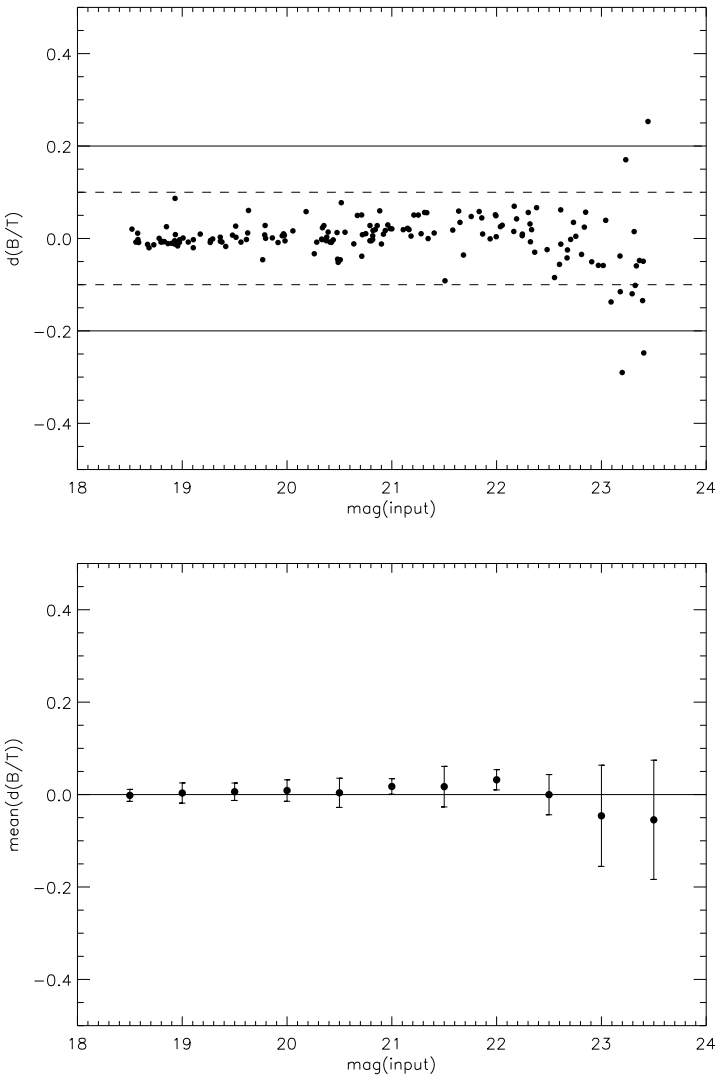

Figure 1. (Top) $d(B/T)$=B/T(measured)–B/T(input) as a function of the input magnitude. (Bottom) Mean d(B/T) vs. input magnitude with 1 σ error bars.

In order to obtain a bulge+disc decomposition of the objects, we fit ellipses to their isoluminosity contours down to 1.5 σ using the task ELLIPSE from IRAF. The surface brightness and ellipticity profiles obtained are used to recover the structural parameters of the galaxies.

3 THE GALAXY CLASSIFICATION PROCEDURE

The classification technique is based on the decomposition of the surface brightness profiles of the galaxies in bulge and disc components. The fitting algorithm is discussed exten-

sively in Trujillo et al (2001b). Here we explain the main points of the routine.

The final surface brightness distributions resulting from the convolution between the PSF and our 2D (i.e. elliptical) model surface brightness distributions are dependent on the intrinsic ellipticity of the original source - as is the case with real data. A key problem remains, which is what value of the ellipticity is choosen to represent the ellipticity of the model. The ellipticity of the isophotes are reduced by seeing. This reduction depends on the radial distance of the isophote to the center of the model, the size of the seeing, and the values of the model parameters. Consequently, to evaluate the intrinsic ellipticity of a model it is often insufficient to simply measure the ellipticity at one given radial distance (e.g. 2 effective radii). To illustrate this, the observed ellipticity at 2 r_e on galaxies which have an effective radius of similar size to the FWHM (these galaxies are common at high redshift) is 30% less than the true ellipticity for galaxies with an exponential profile (n=1), and 45% less for galaxies with a de Vaucouleurs profile (n=4). The use of models with underestimated ellipticity affects the evaluation of the other model parameters, biasing the results. One result of this bias is the estimation of smaller values of index n. This bias increases as the value of n increases (Trujillo et al. 2001a,c).

Consequently, the determination of the intrinsic ellipticity of the source and the fitting process to determine the structural parameters should be done in tandem (i.e. using an iterative and self-consistent routine) and not as two separate tasks. To do this we simultaneously fit both the observed surface brightness and ellipticity profiles using convolved profiles for each (see how the algorithm works in Figure 6 from Trujillo et al. 2001b).

Our 2D fitted galaxy model has two components: a bulge and a disc. The 2D bulge component is a pure Sérsic (1968) profile of the form†:

$$I(\xi) = I_e 10^{-b_n[(\xi/r_e)^{1/n}-1]} \quad (1)$$

where I_e is the effective intensity, r_e is the bulge effective radius and $b_n = 0.868n - 0.142$ (Caon et al 1993). The disc component is an exponential profile given by:

$$I(\xi) = I_o e^{\xi/h} \quad (2)$$

where I_o is the central intensity and h is the exponential disc scale-length. The set of free parameters is completed with the ellipticities of the bulge ϵ_b and the disc ϵ_d. The bulge and disc profiles were convolved with the instrumental PSF of the HST obtained from stellar profiles located on the images. Special attention was paid to this convolution. The real PSFs were fitted by Moffat functions and the convolutions were developed analytically on real space. Also, to avoid the problem of the undersampling of the PSF we average different stellar profiles obtaining a composed median PSF. To this median profile we fit our analytical PSF. We have estimated a ∼5% uncertainty in the estimation of the FWHM due to changes from one WFPC2 position to another. This uncertainty implies an error on the parameters estimation less than 10%.

A Levenberg-Marquardt non–linear fitting algorithm (Press et al 1992) was used to determine the free parameters set which minimizes χ^2. Extensive Monte-Carlo simulations were done in order to check the reliability of the recovered parameters (see Section 4). The surface brightness profiles and ellipticity profiles of each galaxy were fitted at the same time. Each galaxy was fitted by a single Sérsic profile and a Sérsic + exponential profile.

† The surface brightness distribution are explicitily written on elliptical coordinates (ξ, θ) (Trujillo et al. 2001a).

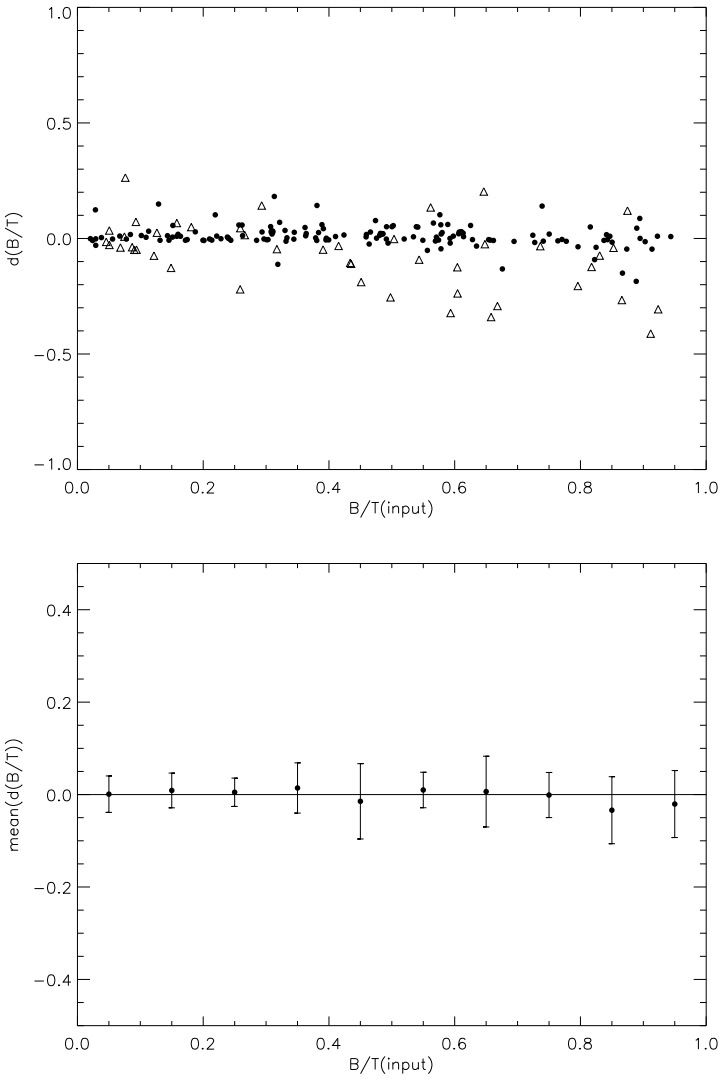

Figure 2. (Top) The difference, d(B/T), between measured and input B/T versus B/T(input) for two different magnitude intervals: $I \leq 23$ (solid circles) and I¿23 (triangles). (Bottom) Mean d(B/T) versus B/T(input) with 1 σ error bars.

Following previous studies (e.g. Marleau & Simard 1998), galaxy classification was based on the bulge to total luminosity ratio, B/T. We consider as "ellipticals" those objects with $B/T > 0.6$, in which case a better fit can be obtained with only one component. The parameters of these objects were taken from the pure Sérsic fitting. Galaxies with B/T between 0.5–0.6 were classified as S0. Finally, objects with $B/T < 0.5$ were classified as "spirals". We consider as "spheroidal" galaxies those with B/T >0.5 as Marleau & Simard (1998). The discrimination between the different types of galaxies was made following the values of B/T given

by Simien & de Vaucouleurs (1986). Quantitative selected ellipticals can be contaminated by galaxies such as compact narrow emission–line objects. These galaxies exhibit high bulge fractions even though they are not real ellipticals. These objects can be ∼15% of the elliptical sample (Im et al. 2001) and their presence must be taken into account at estimating the uncertainty on the ellipticals comoving density parameters‡.

Galaxies selected using only the B/T >0.5 criteria may not all be E/S0s, but could include later galaxy types. To quantify this bias we use the analysis performed by Im et al. (2001) for a local galaxy sample (Frei et al. 1999). Galaxies with T ≤0 (i.e. E/S0s) represent 76% of the local sample selected using B/T >0.5. So, a contamination of ∼ 25% can be expected in the objects that we are labeling as E/S0s at high redshift. However, the contamination for objects with T ≤0 in the objects named "spirals" (i.e. B/T <0.5) is just 8%. Some methods have been identified to remove the bias in the E/S0s selected sample with the use of red colors selected galaxies or the use of low asymmetry objects. However, the first option clearly biases the sample to objects that have a quiet evolution (and what we want is precisely study this hypothesis) and the second has been shown to be inappropriate in objects at high redshift (i.e. low S/N as our objects have) by Conselice, Bershady & Jangren (2000). Despite the known morphological type biases, due to the above reasons we have chosen to maintain the B/T selection criteria as the sole morphological selection criteria.

For the ellipticals, we have also imposed a restriction based on absolute magnitude. By doing this, we have classified a galaxy as "dwarf" when $M_B \geq -17.0$. The absolute magnitudes were obtained after applying the K-correction prescription of Poggianti (1997) assuming (hereafter) a cosmology with H_0=75 km s^{-1} Mpc^{-1}, q_0=0.5, $\Omega_m = 1.0$ and Ω_Λ=0.

Once the automated classification is done, a visual inspection was also made for each object. Some objects are not fitted well by either a pure Sérsic profile or a bulge+disc profile. They were classified as "irregular" galaxies. Those with evidence of mergers (close companions and irregular shapes) were catalogued as "mergers". We also had 4 objects whose best fit is achieved by a pure Sérsic profile with $n \approx 0.5$. It is important to note that the luminosity density of a Sérsic profile with n< 0.5 has a depression in its central part representing an unlikely physical situation (Trujillo et al 2001a). Marleau & Simard (1998) also obtained some objects of this class on the HDF images. The visual morphological shape of these objects is peculiar appearing elongated. Marleau & Simard (1998) claimed that this kind of objects could be remnants of mergers or close tidal disruptions. We have included them into the merger category.

‡ As a matter of caution we also must regard that these "interlopers" are basically placed at high redshift (z>0.8) or they are faint galaxies M_B <-18 (see Im et al. 2001 their Figure 17). For that reason, most of these galaxies are expected to be out of our studied sample.

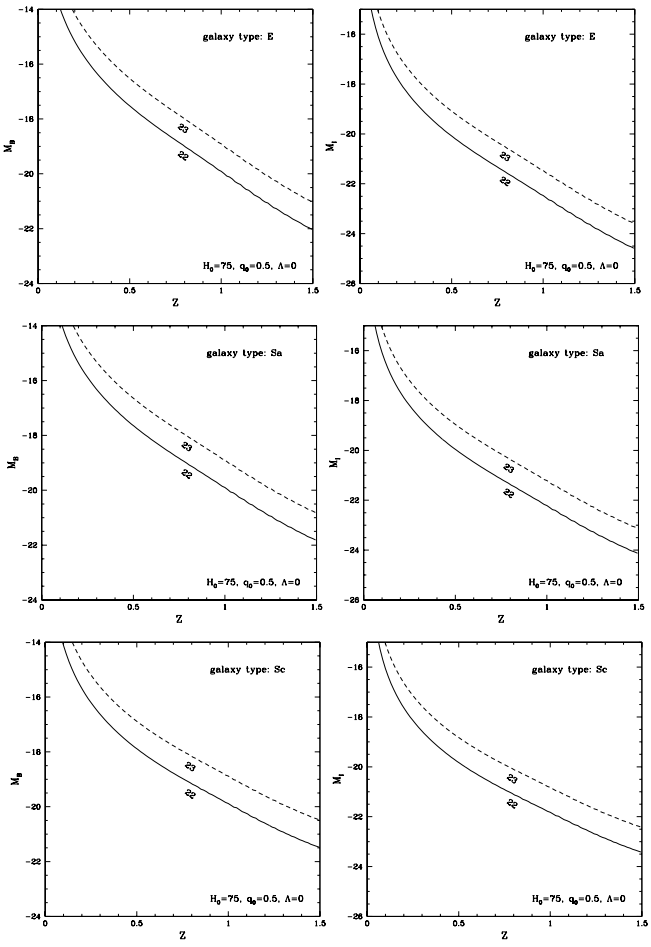

Figure 3. The complete magnitude as a function of the redshift for objects with apparent magnitudes: $I = 22$ (full line) and $I = 23$ (dashed line). Three different kind of objects are represented: ellipticals (top), Sa (middle) and Sc (bottom). See text for details.

4 THE COMPLETENESS OF THE SAMPLE

Since selection effects can mimic evolutionary changes in high redshift objects, it is necessary to achieve a complete unbiased sample of objects. The determination of the completeness of the sample is done in two steps. First, we determine the faintest apparent magnitude down to which the recovered parameters are reliable. In particular, we will focus on the B/T ratio because it is the parameter used for the classification of the galaxies. We evaluated this limiting magnitude by Monte–Carlo simulations of artificial galaxies with similar magnitudes and structural parameters as the real objects. Once this magnitude is obtained, the second step for the completeness of the sample consists in determining how bright (i.e. the absolute magnitude) a galaxy has to be in order to be observed in our whole redshift interval. The limiting absolute magnitude was obtained by using typical spectra from every type of objects, which allows us to verify that we are studying the same kind of objects in all redshift intervals. Unfortunately, most previous studies

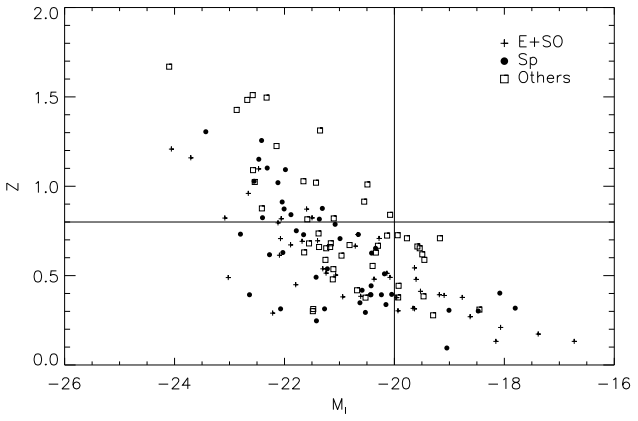

Figure 4. The $M_I - z$ diagram for the galaxies detected at the SSA13 and SSA22 fields. The absolute magnitudes have been computed for a $H_o = 75 kms^{-1}Mpc^{-1}$, $\Omega_m = 1$ and $q_o = 0.5$ cosmology.

of the structural properties of high redshift samples do not determine their limiting absolute magnitudes. This type of samples are obtained with only an apparent limiting magnitude, which biases the sample to the brightest objects at high redshifts. For this reason, it is necessary to use a sample cut by absolute magnitude.

4.1 Monte-Carlo simulations

We performed Monte–Carlo simulations to test the reliability of our method. First, we tested the ability to recover parameters from bulge–only (i.e. purely elliptical) structures, and second we explored the possibility of carrying out accurate bulge+disc decompositions. In both cases we created 150 artificial galaxies with structural parameters randomly distributed in the following ranges:

- bulge–only structures: 19≤I≤23, $0.05'' \leq r_e \leq 0.6''$, $0.5 \leq n \leq 4$, and $0 \leq \epsilon \leq 0.6$ (the lower limit on n is due to the physical restrictions pointed out in Trujillo et al 2001a).
- bulge+disc structures: 18.5≤I≤23.5, $0.05'' \leq r_e \leq 0.6''$, $0.5 \leq n \leq 4$, and $0 \leq \epsilon_b \leq 0.4$, 0.2"$\leq h \leq 1.5''$, $0 \leq B/T \leq 1$, and $0 \leq \epsilon_d \leq 0.6$.

The artificial galaxies were created by using the IRAF task MKOBJECT. We support as an input to this task

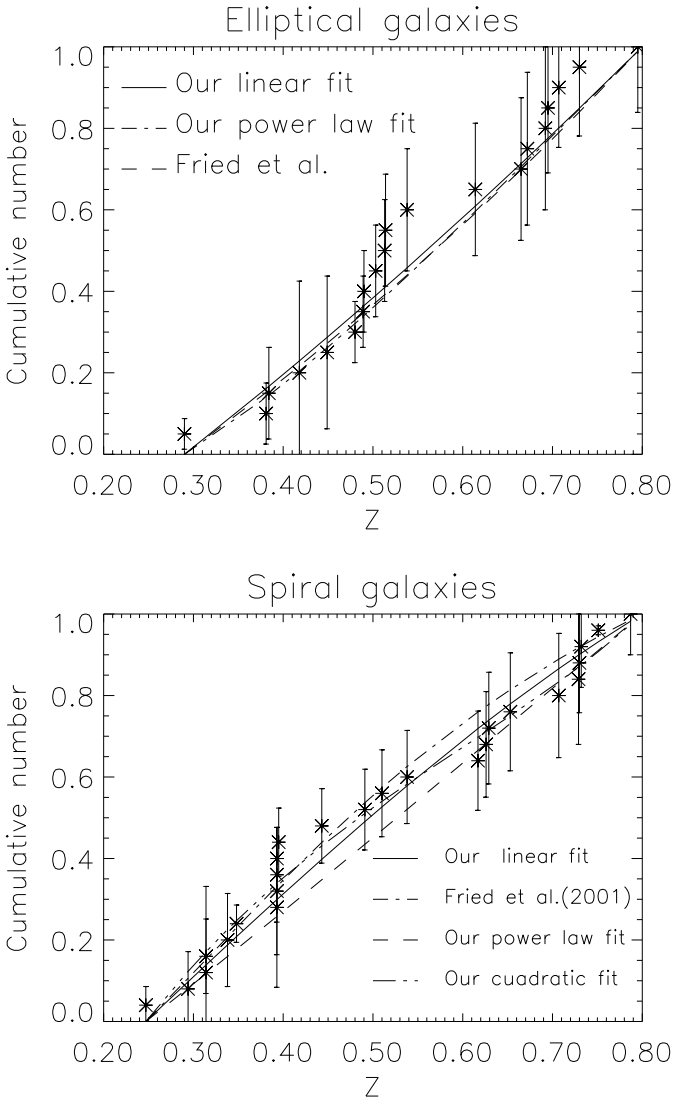

Figure 5. The cumulative number distribution function of E/S0s (top) and spirals (bottom) as a function of the redshift. The best fits derived from linear and quadratic comoving densities are overplotted. It is also showed the cumulative distributions derived from Fried et al. (2001). See text for more details.

the surface brightness distribution coming from our detailed convolution between the PSF and the original model. To simulate the real conditions of our observations, we added a background sky image (free of sources) taken from a piece of the real image; the dispersion in the sky determination was 0.1 %. The PSF FWHM in the simulation was set at $0.2''$ and assumed known exactly. The pixel scale of the simulation was $0.1''$, as is the real WFPC2 pixel size. The same procedure was used to process both the simulated and the actual data.

Figure 1 shows $d(B/T)$=B/T(measured)–B/T(input) as a function of the input magnitude. For galaxies brighter than $I = 23$ magnitude $d(B/T)$ is less than 0.1. This is a very accurate determination of this parameter. Figure 2 shows $d(B/T)$ as a function of the $B/T(input)$. Objects with $I \geq 23$ (triangles) have bigger dispersion of $d(B/T)$ than ob-

Table 1. Galaxies from SSA13 with $I \leq 23.0$.

ID	Z	M_I	B/T	ID	Z	M_I	B/T
5	0.612	-20.96	-1.00	67	0.270	-18.62	1.00
10	0.554	-20.39	-1.00	69	0.317	-19.66	1.00
11	1.225	-22.14	-1.00	70	0.314	-21.27	0.32
12	0.489	-23.02	0.54	71	0.210	-18.06	1.00
14	0.667	-20.29	-1.00	72	0.876	-21.31	0.05
16	1.614	-28.14	1.00	75	0.818	-22.06	1.00
18	0.491	-21.42	0.20	78	0.490	-20.08	1.00
19	0.393	-20.42	0.03	87	1.427	-22.86	-1.00
20	1.028	-21.65	-1.00	100	0.377	-20.52	-1.00
21	0.443	-20.42	0.10	101	1.256	-22.41	0.32
25	0.730	-20.65	0.03	103	0.629	-22.02	0.31
28	0.736	-21.38	-1.00	105	0.395	-20.04	0.40
31	1.090	-22.57	-1.00	107	0.314	-19.63	1.00
32	0.278	-19.29	-1.00	108	0.680	-21.55	-1.00
36	0.338	-20.15	0.25	109	0.393	-20.43	0.30
37	1.020	-21.42	-1.00	110	0.660	-21.17	-1.00
38	0.393	-20.23	0.28	111	0.729	-21.65	0.07
39	0.449	-21.79	1.00	113	0.629	-20.33	-1.00
41	0.480	-20.37	0.57	114	0.660	-21.37	-1.00
43	1.305	-23.43	0.34	115	0.389	-19.09	0.52
46	0.820	-21.10	-1.00	116	0.630	-21.64	-1.00
47	0.732	-22.80	0.44	120	0.841	-21.88	0.02
52	0.914	-20.54	-1.00	122	0.503	-21.06	1.00
55	1.028	-22.55	0.22	124	0.393	-22.63	0.16
59	1.483	-22.67	-1.00	127	0.393	-19.18	1.00
61	0.310	-18.45	-1.00	155	0.730	-20.66	0.57
62	0.314	-22.07	0.43	171	0.726	-19.94	-1.00
64	0.681	-21.15	-1.00	174	0.479	-19.60	1.00

Table 2. Galaxies from SSA22 with $I \leq 23.0$.

ID	Z	M_I	B/T	ID	Z	M_I	B/T
9	1.093	-21.98	0.04	80	1.669	-24.09	-1.00
11	0.626	-20.41	0.19	81	0.384	-19.47	-1.00
13	0.653	-20.34	0.34	82	0.384	-20.61	1.00
14	0.538	-21.30	1.00	83	0.510	-20.18	0.12
19	0.294	-20.52	0.14	87	0.306	-19.00	0.47
20	0.663	-19.58	-1.00	89	1.151	-22.46	0.41
28	0.247	-21.41	0.04	90	0.412	-19.52	1.00
30	0.751	-21.78	0.34	91	0.513	-20.13	1.00
32	1.024	-22.54	-1.00	92	0.381	-20.94	0.50
33	0.707	-22.07	1.00	93	0.377	-19.95	1.00
38	1.208	-24.05	1.00	96	0.290	-22.21	1.00
44	0.672	-21.88	0.51	100	0.303	-19.93	1.00
45	0.132	-18.15	0.53	102	0.824	-22.39	0.20
46	0.912	-22.04	0.08	103	1.159	-23.70	1.00
47	0.173	-17.38	1.00	108	0.588	-21.25	-1.00
49	0.707	-20.98	0.37	111	0.302	-18.47	0.21
50	0.538	-21.22	0.09	118	0.816	-21.36	0.36
51	0.536	-21.11	-1.00	123	0.095	-19.04	0.11
54	0.418	-20.67	-1.00	124	0.671	-20.81	-1.00
55	0.815	-21.58	-1.00	125	0.873	-22.00	0.24
56	0.318	-17.80	0.23	127	0.695	-21.39	1.00
59	0.418	-20.58	0.50	143	1.102	-22.31	0.09
60	1.392	-19.54	-1.00	147	0.514	-21.24	1.00
67	0.588	-19.45	-1.00	148	0.876	-22.41	-1.00
69	0.692	-21.67	1.00	150	0.795	-22.11	1.00
70	0.348	-20.62	0.38	152	0.617	-22.27	0.17
71	0.132	-16.72	1.00	154	0.614	-22.09	1.00
72	0.787	-21.07	0.07	155	0.665	-20.71	1.00
73	0.822	-23.08	1.00	161	0.960	-22.65	1.00
75	0.724	-20.13	-1.00	166	0.378	-18.76	1.00
77	1.020	-22.11	0.36	172	0.378	-19.93	-1.00
78	0.823	-21.49	0.55	204	0.709	-19.77	-1.00

jects with $I \leq 23$ (points). From our simulations it follows that $I = 23$ is the limiting magnitude for reliable recover of the B/T parameter. The limiting magnitude for the rest of structural parameters will be studied in a forth–coming paper. To our limiting apparent magnitude, the sample of galaxies is reduced to 120 galaxies. According to their B/T ratio, absolute magnitude and visual inspection (see Section 3), they were classified as: ellipticals (26), dwarfs (6), S0 (9), irregulars (20), mergers (17) and spirals (42). This left us with $\sim 34\%$ spheroidal galaxies (E+Dwarfs+S0), $\sim 35\%$ spirals and $\sim 31\%$ of unclassified objects. Tables 1 and 2 show the B/T ratios (column 4) and M_I (column 3) for the 120 galaxies with $I \leq 23.0$ for the SSA13 and SSA22, respectively. These tables also show the identification number (column 1) and the redshift of the objects (column 2) given by Cowie et al (1996). Galaxies classified as ellipticals and dwarfs have $B/T = 1.0$, those classified as irregular of mergers have been marked with $B/T = -1.0$.

4.2 Completeness as function of redshift

In order to be sure that we are studying the same kind of objects at different redshifts we must determine the absolute limiting magnitude of our sample. On doing this we avoid biasing our sample to brighter objects at high redshift. Some claims of galactic evolution have been a consequence of this bias. As an example, Simard et al (1999) analyzed the problem of the completeness of the sample. If selection effects were ignored in their galaxies, then the mean disc surface brightness increases by ≈ 1.3 magnitudes from $z = 0.1$ to $z = 0.9$. Most of this evolution is plausibly due to comparing low–luminosity galaxies in nearby redshift bins to high-luminosity galaxies in distant bins. If this effect is taken into account, no discernible evolution remains in the disc surface brightness of their disk dominated galaxies. In order to avoid this kind of problem it is necessary to make a selection of the objects on the basis of their absolute luminosity.

Given our apparent limiting magnitude of $I = 23$, we have studied the completeness of our sample for three different class of galaxies: Sa, Sc and E. Figure 3 shows, for a limiting magnitude of I=23 , the absolute magnitude down to which a galaxy can be observed as a function of z. This figure was generated using spectral models of 15 Gyr old galaxies (Poggianti 1997). For our distribution of 120 objects with $I \leq 23$, the parameters which maximize the number of objects into a complete sample are $z \leq 0.8$ and $M_I \leq -20.0$ ($M_B \leq -18$)[§]. This left us with a total of 61 objects: 20 E/S0, 25 spirals, 16 irregulars and mergers, or equivalently:$\sim 33\%$ E/S0 $\sim 41\%$ spirals and $\sim 26\%$ unclassified objects. Figure 4 shows the $M - z$ diagram for our whole sample down to $I \leq 23$. The complete subsample studied (left-down corner) is enclosed by the horizontal and vertical lines. This kind of selection criteria is similar to that used by Simard et al (1999) and Fried et al (2001).

[§] We have repeated this calculation with the starburst galaxy NGC4449 without finding any substantial difference.

5 RESULTS AND DISCUSSION

5.1 Galaxy classification

There is no substantial differences between the fraction of galaxies which correspond to the different classes when the sample is restricted in apparent and absolute magnitude. We must note that these numbers are in good agreement with the percentage of E/S0 given by visual classification systems (van den Bergh et al 1996, 2000) in the HDF, but are quite different from that given automated classification of Marleau & Simard (1998), 8%. The classification of Marleau & Simard (1998) takes into account all objects with $I_{814} \leq 26$ from the HDF. They claim that the discrepancy with visual classifications is due to the difference in the classification of small round galaxies with half-light radii less than $0.''31$. Visually these galaxies are classified as elliptical galaxies, Marleau & Simard classify them as disc–dominated systems with bulge fractions less than 0.5. But, galaxies with an intrinsically big B/T tends to be systematically obtained with lower values of B/T in their automated routine (see Fig. 10 of Marleau & Simard 1998). The ellipticals in the HDF which have been (probably) mis–classified by these authors are those principally coming from the fainter subsample. Although the relation between the B/T output of their simulation and the input magnitude of the objects is not provided by these authors (and consequently our assertions must be taken with caution), it is certainly possible that B/T results stronger affected at increasing the input magnitude (i.e. at lower signal ratios), and for that reason, the high redshift population of elliptical galaxies remains biased. By using an automated procedure which avoids this problem we have been able to obtain a result similar to van den Bergh et al (1996, 2000).

Interestingly, our sample and the HDF one are imaging a galaxy population centered around $z \sim 0.5$, the principal difference being in the exposure time. Because of the different depth in the images, substantial differences would be expected for the fainter subpopulation (smaller and irregular galaxies) between our sample and those based on the HDF. In fact, in the HDF apparent magnitude–limited sample contains 39% of unclassified objects whereas we obtain $\sim 30\%$.

5.2 Galaxy evolution

The two main models of galaxy evolution (monolithic collapse and hierarchical clustering) present a completely different scenario of galaxy evolution, so that the observational implications also are very different. One of these concerns the comoving density of the galaxies. In the redshift interval studied, the hierarchical model framework proposes the comoving density of big galaxies (E/S0s and spirals) decrease with redshift, being constant in the monolithic model. We have computed the comoving density $\rho(z)$ for these two different types of galaxies in our complete subsample.

We have assumed both a linear function for modeling the comoving density,

$$\rho(z) = a + bz \tag{3}$$

with a=$\rho(0)$ the comoving density at z=0 and b=$(\rho(z_{max}) - \rho(0))/z_{max}$ with z_{max} the maximum value which z reaches in our limiting subsample, and a power law of the form:

$$\rho(z) = a(1+z)^b \tag{4}$$

with a=$\rho(0)$ the comoving density at z=0.

To reduce the loss of information in our data we avoid binning them. The values of the parameters of the function $\rho(z)$ are achieved by running a Kolmogorov-Smirnov test between the cumulative probability distribution function of finding a galaxy inside our imaging solid angle at a given z given $\rho(z)$ and the cumulative distribution from the real data. The cumulative probability function for our model is computed as:

$$P(z) = \frac{\int_{z_{min}}^{z} \rho(z')r^2(z')(dr/dz)dz'}{\int_{z_{min}}^{z_{max}} \rho(z')r^2(z')(dr/dz)dz'} \tag{5}$$

where z_{min} is the closest galaxy redshift, z_{max}=0.8 for our limiting subsample and r(z) is the comoving distance to an object placed at z.

The Kolmogorov-Smirnov (KS) test gives the probability that two data sets come from the same distribution. The best comoving density is that which maximize this probability.

As a matter of caution, we must note that E/S0 galaxies are placed preferentially in high density environments, being more strongly clustered than other types of galaxies. In order to evaluate the effect of clustering in our comoving density, we have studied the contribution of the E/S0 galaxies of each field to our cumulative function. The number of galaxies on the regions of more accumulation (0.48-0.54 and 0.69-0.73) come from both fields with approximately the same contribution, rejecting a clustering explanation.

To evaluate the errors on the parameters in the E/S0 and in the spiral sample we have assumed that a least two galaxies in each sample are misclassified. This represents $\sim$10% of each sample. We construct all the subsamples that can be obtained by removing two elements on the original samples and then we recover the values of the parameters associated to them. Using these values we estimate the median and the standard deviation. These are the numbers that we present as the parameter estimations and the errors associated to these measurements. Fig. 5 shows the original whole sample (i.e. without removing any point) and overplotted is the cumulative function associated with the parameters measured as explained before. Bar errors in Fig. 5 were estimated by measuring at each point the maximum distance between the cumulative function represented by using the whole sample and all the cumulative functions resulting from the previous subsamples. We have also overplotted the cumulative distribution obtained from the comoving densities fitted by Fried et al. (2001), who have a similar absolute magnitude cut for their sample ($M_B \leq -18.5$).

The comoving density of the E/S0s which gives a maximum probability in the KS test for a linear form is given by: $\rho(z) = 0.0033(\pm 0.0015) - 0.0015(\pm 0.0010) \times z$. The KS probability of this density is 0.90. This comoving density is closer to that deduced by Fried et al (2001). Using their fit to our sample we obtain a KS p (KS p_F) of 0.87. The number of E/S0s decreases with redshift. For the cosmology chosen, this decrease is $\sim 45(\pm 30)\%$. At using the power–law model, the KS probability is slightly better, 0.92. We have:

[!htb]

Table 3. Parameters of the comoving density. H_0=75kms^{-1}Mpc^{-1}

Model	Type	a	b	c	KS p	KS p_F
		$\Omega_m = 1$		$\Omega_\Lambda = 0$		
a+b×z	E/S0	0.0033(±0.0015)	-0.0015(±0.0010)	-	0.90	0.87
a×(1+z)^b	E/S0	0.0039(±0.0018)	-1.6(±0.4)	-	0.92	-
a+b×z	S	0.0069(±0.0025)	0.0014(±0.0006)	-	0.78	0.70
a×(1+z)^b	S	0.0060(±0.0031)	1.7(±0.5)	-	0.92	-
a+b×z+c×z^2	S	0.0095(±0.0036)	0.0027(±0.0012)	-0.0031(±0.0018)	0.96	-
		$\Omega_m = 0.3$		$\Omega_\Lambda = 0.7$		
a+b×z	E/S0	0.0049(±0.0026)	0.0032(±0.0040)	-	0.86	0.83
a×(1+z)^b	E/S0	0.0055(±0.0024)	-1.1(±0.3)	-	0.82	-
a+b×z	S	0.0071(±0.0022)	-0.0019(±0.0027)	-	0.81	0.73
a×(1+z)^b	S	0.0043(±0.0025)	1.5(±0.4)	-	0.85	-
a+b×z+c×z^2	S	0.0063(±0.0042)	0.0017(±0.0011)	-0.0012(±0.0015)	0.87	-

$\rho(z) = 0.0039(\pm0.0018) \times (1+z)^{-1.6(\pm0.4)}$. In this case, the decrease of elliptical galaxies is $\sim 60(\pm10)\%$. This behavior is in a very good agreement with the prediction from the hierarchical clustering scenario for this cosmology (Baugh et al. 1996; Kauffmann et al. 1996) but differs from the results presented in Totani & Yoshii (1998) and Im et al. (2001). Interestingly, Daddi (2001) has pointed out that strong discrepancies in the number density evolution for the EROs (Extremely Red Objects¶) can be understood in terms of cosmic variance: "it is much probable, on average, to underestimate the true ERO surface density with small area surveys". Maybe a similar explanation also holds for more modest redshift E/S0 population and this can be of help to understand the discrepancies in the number density evolution pointed out for different authors.

For the spirals, the comoving density is $\rho(z) = 0.0069(\pm0.0025) + 0.0014(\pm0.0006) \times z$, but the KS probability is just 0.78. The parameters of the power–law model for this family are $\rho(0) = 0.0060(\pm0.0031)$ and m=1.7(±0.5) with a KS probability of 0.92. Interestingly, for this population a peak in the range $z = 0.4 - 0.5$ is shown in the comoving density obtained from binned data in Fried et al. (2001), although they fit only a linear comoving density. Probing on this possibility, we have also tested a quadratic comoving density:

$$\rho(z) = a + bz + cz^2 \quad (6)$$

where the interpretation of these parameters is as follows: a=$\rho(0)$, b=$2\triangle\rho/z_p$ where z_p is the redshift where the comoving density reaches its biggest value and $\triangle\rho = \rho(z_p) - \rho(0)$ and c=-$\triangle\rho/z_p^2$. Using a quadratic comoving density we obtain the highest probability, 0.96, with the next values for the parameters: $\rho(z) = 0.0095(\pm0.0036)+0.0027(\pm0.0012)\times z - 0.0031(\pm0.0018) \times z^2$. Notice that this implies a peak of the density at $z = 0.43$. Nevertheless, the value of the comoving density at this peak is just 6% higher that at $z = 0$. Meanwhile the value of the density at $z = 0.8$ is slightly higher (about 1%) than at $z = 0$. Consequently, contrary to the E/S0s, brighter spiral galaxies ($M_B \leq -18$) seem to have a relatively quiet evolution.

Our values of $\rho(0)$ for E/S0 and spiral galaxies are in good agreement with the values that can be obtained by using the fit to the Schechter luminosity function (Schechter 1976) of nearby samples (Marzke et al. 1998). For $M_B \leq -18$, the local comoving density is $\rho(0)=0.0026 \pm 0.0007$ (E/S0s) and $\rho(0)=0.0054 \pm 0.0014$ (spiral galaxies).

We have also evaluated the previous quantities assuming a different cosmology: $\Omega_m = 0.3$ and $\Omega_\Lambda = 0.7$. In this case, our absolute magnitude limit is $M_B \leq -19$. We summarize our results in Table 3. The E/S0 comoving density at this cosmology seems to no–evolve or slightly decreases. This is a similar result to that obtained for this cosmology by Totani & Yoshii (1998) and Im et al. (2001) and what it is expected from semi–analytical hierarchical models (e.g. Kauffmann & Charlot 1998). The results for the spiral galaxies are compatible with no number density evolution.

6 CONCLUSIONS

We present quantitative morphology of galaxies in two Hawaiian Deep Fields imaged by 6 HST fields. Down to the limiting magnitude of our sample, nearly all galaxies have spectroscopic redshifts. The morphology has been obtained by fitting a pure Sérsic and Sérsic + exponential profiles to the surface brightness distribution of the galaxies. Monte-Carlo simulations have been carried out in order to determine the limiting magnitude down to which the recovered structural parameters are reliable. The galaxies have been classified according to the B/T ratio. E/S0s systems are those with $B/T > 0.5$. Our simulations suggest an apparent magnitude limit of I=23. We have also accurately determined the absolute limiting magnitude of our sample $M_B \leq -18$. The complete subsample is composed by 61 objects up to $z = 0.8$.

The percentage of the different galaxy types in the whole sample are in good agreement with those obtained in the HDF by visual methods. We have computed the comoving density of the galaxies as function of redshift. For an Einstein–de Sitter universe, the comoving density of E/S0s

¶ Most of these objects are expected to be E/S0s at redshift 1≤z≤2.

decreases as z increases, in very good agreement with the predictions of hierarchical clustering models of galaxy evolution. The comoving density of spiral galaxies shows a good fit to a quadratic form: it grows a $\sim$6% from $z = 0$ until $z = 0.43$, and then decreases slightly until $z = 0.8$. This fit is compatible with no number evolution. For open or Λ universes, the E/S0 galaxies comoving density is compatible with no number density evolution or a slightly decrease as it is expected from semi–analytical models in hierarchical clustering scenarios. Density comoving for brighter spiral galaxies also remain quite constant at this redshift range.

ACKNOWLEDGMENTS

We wish to thank David Cristóbal and Juan Betancort for valuable discussions. We are also indebted to Victor Debattista who kindly proofread versions of this manuscript. The authors are grateful to the anonymous referee for the valuable suggestions that helped us to improve the rigor and clarity of this paper.

Based on observations with the NASA/ESA *Hubble Space Telescope* obtained at the Space Telescope Science Institute, which is operated by the Association of Universities for Research in Astronomy, Inc., under NASA contract 5-26555.

REFERENCES

Abraham R. G., Tanvir N. R., Santiago B. X., Ellip R. S., Glazebrook K. & van den Bergh S., 1996, MNRAS, 279, L47.
Baugh C., Cole S. & Frenck C., 1996, MNRAS, 283, 1361.
Bertin E. & Arnout S., 1996, A&AS, 117, 393.
Brinchmann J. et al., 1998, ApJ, 499, 112.
Caon N., Capaccioli M., D'Onofrio M., 1993, MNRAS, 265, 1013.
Conselice C.J., Bershady M.A., Jangren A., 2000, ApJ, 529, 886
Cowie L. L., Gardner J. P., Hu E. M., Songaila A., Hodapp K. W. & Wainscoat R. J., 1994, ApJ, 434, 114.
Cowie, L. L., Hu, E. M. & Songaila, A., 1995, AJ, 110, 1576.
Cowie L. L., Songaila A. & Hu E. M., 1996, AJ, 112, 839.
Daddi E., 2001, Ap&SS, 277, 531
Eggen O. J., Lynden-Bell D. & Sandage A., 1962, ApJ, 136, 748.
Frei, Z., Guhathakurta, P. Gunn, J.E., & Tyson, J.A. 1996, AJ, 111, 1
Fried J. W. et al., 2001, A&A, 367, 788.
Im M. et al., 2001, ApJ, in press.
Kauffmann G., White S. & Guiderdoni B., 1993, MNRAS, 264, 201.
Kauffmann G., Charlot, S. & White S.D.M., 1996, MNRAS, 283, L117
Kauffmann G. & Charlot, S., 1998, preprint (astro–ph/9810031)
Kauffmann G., 1996, MNRAS, 281, 478.
Larson R. B., 1975, MNRAS, 166, 585.
Le Fevre O. et al. 1999, MNRAS, 311, 565.
Marleau F. R. & Simard L., 1998, ApJ, 507, 585.
Marzke, R., da Costa, L.N., Pellegrini, P.S., Willmer, C.N.A., & Geller, M.J., 1998, ApJ, 503, 617
Poggianti B. M., 1997, A&AS, 122, 399.
Press W. H., Teukolsky S. A., Vetterling W. T. & Flannery B. P., 1992, Numerical Recipes (Cambridge: Cambrige Univ. Press).
Prieto M., Aguerri J.A.L., Varela A.M., Munoz-Tunón C., 2001, A&A, 267, 405.
Schade D., Lilly S., Le Fevre O., Hammer F. & Crampton, 1996, ApJ, 464, 79.
Schade D. et al., 1999, ApJ, 525, 31.
Schechter, P., 1976, ApJ, 203, 297.
Sérsic J. 1968. Atlas de Galaxias Australes. (Córdoba: Obs. Astronómico)
Simien F. & de Vaucouleurs G., 1986, ApJ, 302, 564.
Songaila A., Cowie L. L., Hu E. M. & Gardner J. P., 1994, ApJS, 94, 46.
Trujillo I., Aguerri J. A. L., Cepa J. & Gutiérrez C. M., 2001a, MNRAS, 321, 269.
Trujillo I., Aguerri J. A. L., Gutiérrez C. M. & Cepa J., 2001b, AJ, 122, 38.
Trujillo I., Aguerri J. A. L., Gutiérrez C. M. & Cepa J., 2001c, MNRAS, 328, 977.
Totani T. & Yoshii Y., 1998, ApJ, 501, L177
van den Bergh S., Abraham R. G., Ellip R. S., Tanvir N. R., Santiago B. X. & Glazebrook K., 1996, AJ, 112, 359.
van den Bergh S., Cohen J. G., Hogg D. W. & Blandford R., 2000, AJ, 120, 2190.
White S. & Rees M., 1978, MNRAS, 183, 341.

This paper has been produced using the Royal Astronomical Society/Blackwell Science LaTeX style file.

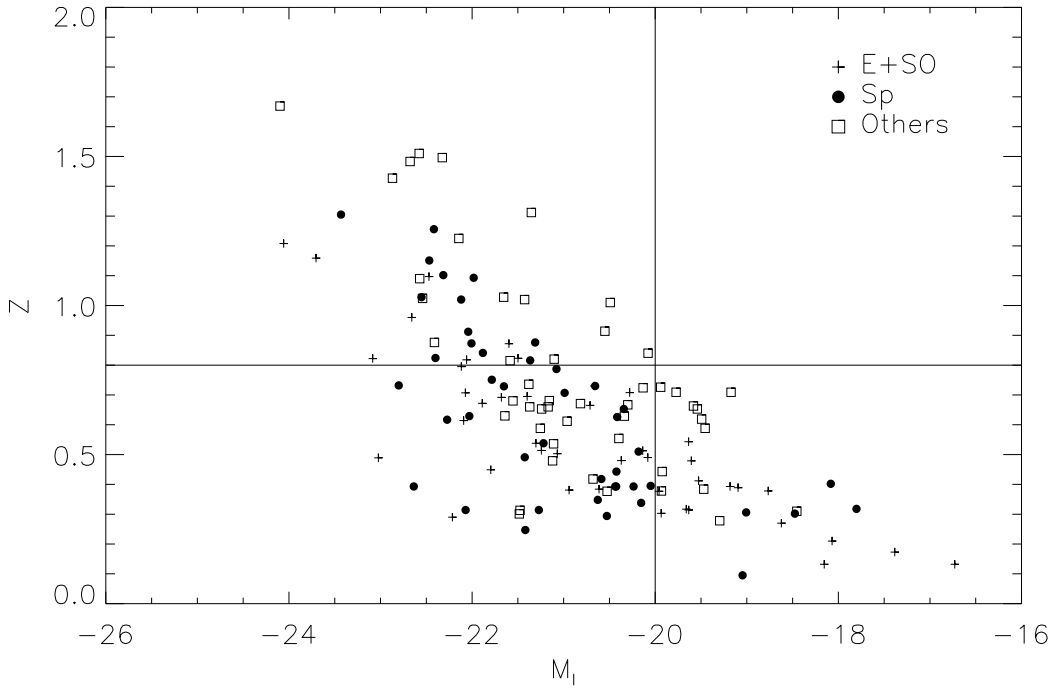
2.0
1.5
1.0
0.5
0.0
Z
−26
−24
−22
−20
−18
−16
M_I
E+SO
Sp
Others